Progress In Electromagnetics Research M, Vol. 65, 91–100, 2018

Design of Frequency Selective Absorber Based on Parallel *LC* Resonators

Kunzhe Zhang*, Wen Jiang, Junyi Ren, and Shuxi Gong

Abstract—This paper describes a method of designing Frequency Selective Absorber (FSA) which has a transmission band between two neighboring absorption bands. The proposed FSA is composed of a lossy layer on the top and a lossless layer at the bottom. The transmission characteristic is produced by the parallel LC resonators embedded in the lossy layer while the absorption ability is realized by the lumped resistors constructed in the lossy layer. An equivalent circuit model (ECM) is developed and discussed for a better understanding of this method. An FSA prototype is fabricated and measured for demonstration. Experiments show that the proposed FSA has a transmission band at the center frequency of 8.14 GHz, which agrees well with simulation. Both transmission and refection coefficients from 4.5 GHz to 7.5 GHz and from 9.1 GHz to 11.3 GHz are under −10 dB, which indicate good absorption in these frequency bands. In addition, the performance of the proposed FSA demonstrates a low sensitivity with respect to the polarization of incident EM waves and is maintained well when the incident angles range from 0° to 45°.

1. INTRODUCTION

Frequency selective surface (FSS) shows a wide range of applications in electromagnetic shielding [1], satellite communication [2], metamaterials fabrication [3] and radar cross section (RCS) reduction [4–6] according to its spatial filter characteristics such as bandpass or bandstop response to electromagnetic (EM) waves [7]. Bandpass FSS (BPFSS) is more widely used among these situations. For example, stealthy radomes based on BPFSS [8] play an extremely important role in stealth aircraft. These radomes can reflect incident EM waves outside the passband to other directions to avoid specular reflection and realize monostatic RCS reduction. However, the reflected EM waves may result in a big increase in bistatic RCS in the reflection direction. In order to reduce both monostatic and bistatic RCSs outside the passband and maintain the transmission characteristic in passband, the concept of frequency selective absorber (FSA) was introduced in [9]. FSA can be seen as a combination of BPFSS and radar absorber (RA). EM waves in the passband could pass through while that outside the passband would be absorbed. The behavior of absorbing rather than reflecting makes it possible to fulfil a low RCS. Since the unique characteristic of FSA, it can be seen as a substitute of bandpass FSS in stealthy radome manufacture. In addition, it can also play an important role in electromagnetic compatibility (EMC) among different systems.

In general, FSA is composed of a lossy layer on the top and a BPFSS at the bottom, as shown in Fig. 1. BPFSS can be identified as a metal plate at the frequency outside the passband. Together with the lossy layer above, the FSA can be recognized as a circuit analog absorber (CAA) [7] and realize absorbing. However, when in the passband, BPFSS is transparent to EM waves, and the CAA model would no longer exist. As a result, EM waves can pass through. Several designs were reported about

Received 9 January 2018, Accepted 26 February 2018, Scheduled 3 March 2018
* Corresponding author: Kunzhe Zhang (zhangkunzhe@hotmail.com).
The authors are with the National Key Laboratory of Antennas and Microwave Technology, Xidian University, Xi'an, Shaanxi 710071, China.

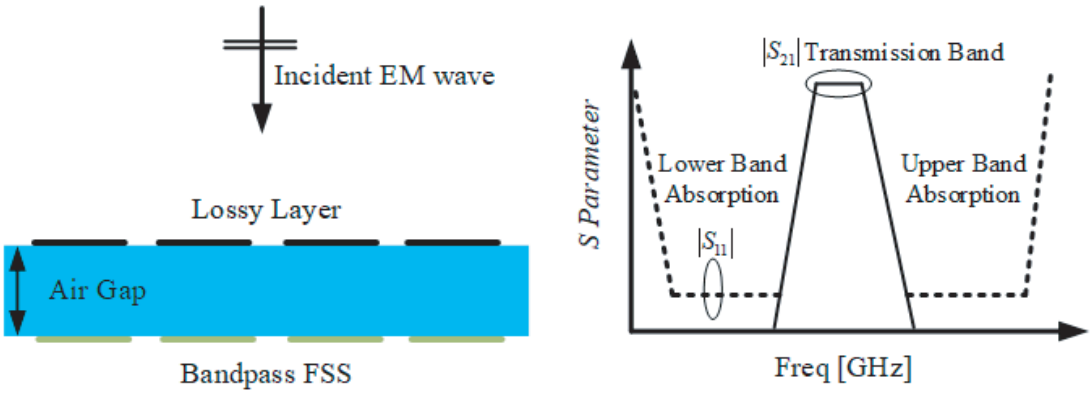

Figure 1. Geometry of FSA and its filter characteristic.

the FSA. However, most of them are structures with lower absorption band and upper transmission band [10–12]. The others are with lower transmission band and upper absorption band [13–15]. A few articles have reported structures whose transmission band located between two absorption bands [16–18]. The main challenge of designing such a type of FSA is how to achieve transmission and alleviate insertion loss in the lossy layer. In past, the main method was to arrange series LC resonators in parallel with lumped resistors in the lossy layer. These series LC resonators resonated at the frequency of BPFSS. When in passband, the induced current would flow through resonators instead of resistors. As a result, the transmission performance could be obtained. However, this method has a disadvantage that additional bias networks are needed to place the resonators, and this would be cumbersome in designing a compact structure.

In this paper, a new method of designing FSA is proposed and investigated. It is implemented by arranging parallel LC resonators in the lossy layer. The advantage of this method is that the parallel LC resonators can be easily integrated in the unit cell without the need for an additional bias network. In addition, the proposed FSA has a superior performance with respect to EM wave's polarizations, stable for oblique incidence and efficient for both monostatic and bistatic RCS reduction. The paper is organized as follows. The process of designing FSA is presented and discussed in Section 2. In Section 3, the performance of the designed FSA and its advantage in bistatic RCS reduction are introduced. Fabrication details and experiment setup are described in Section 4. Conclusions are drawn in Section 5. All simulations in this paper are accomplished by using the advanced system design (*ADS*) and High Frequency Solution Solver (*HFSS*).

2. PROCESS OF DESIGNING FSA

2.1. Principle of Selecting Parallel LC Resonator

As mentioned above, the key to design the FSA is how to make the lossy layer become transparent to EM waves at the frequency of passband while maintaining low insertion loss. To achieve this purpose, tic-tac-toe grids (TTTG) are proposed and investigated, as shown in Fig. 2(a). They are printed on a thin dielectric substrate F_4BM with a permittivity $\varepsilon_r = 3.5$ and thickness of 0.5 mm. The reasons for choosing TTTG are that it has a simple structure and is insensitive to the polarization of the incident EM waves as well as easy to be integrated with the lumped resonators. Fig. 3 shows the simulation results obtained from *HFSS*. As can be seen, the TTTG has a bandstop response around the TZ frequency at normal incidence. However, when parallel LC resonators resonating at TZ frequency are constructed in TTTG unit, as shown in Fig. 2(b), its filter characteristic would be quite different. As can be seen from the simulation results in Fig. 3, the obtained TTTG shows a bandpass response at TZ frequency. This phenomenon can be interpreted from the point view of induced current. The impedance of LC resonators would be infinite at TZ frequency, so the branch of TTTG is divided into two short parts. Slight current would be induced upon them. As a result, TTTG would become transparent to EM waves.

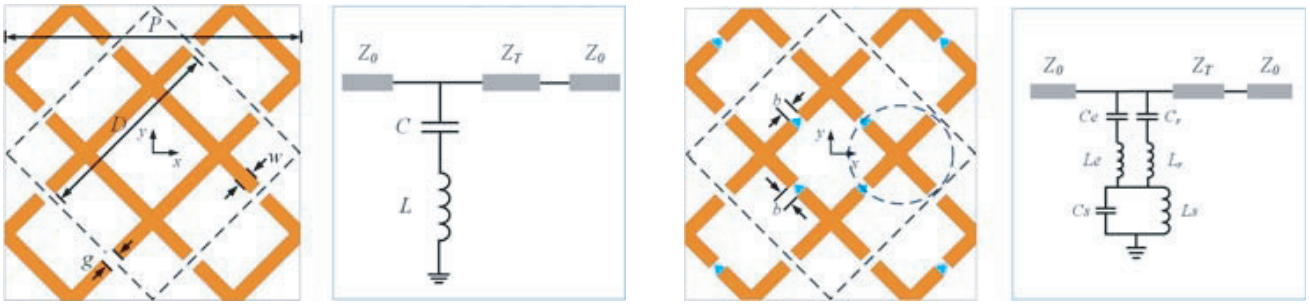

(a) (b)

Figure 2. Top view of the TTTG unit cell and its ECM in (a) original situation and (b) with LC resonators loaded. $P = 25\,\text{mm}$, $g = 1.2\,\text{mm}$, $D = 16.5\,\text{mm}$, $w = 1.2\,\text{mm}$, $b = 0.4\,\text{mm}$, $L = 6.61\,\text{nH}$, $C = 0.06\,\text{pF}$, $Le = 4.58\,\text{nH}$, $Ce = 0.08\,\text{pF}$, $Lr = 6.45\,\text{nH}$, $Cr = 0.06\,\text{pF}$, $Ls = 0.66\,\text{nH}$, $Cs = 0.6\,\text{pF}$.

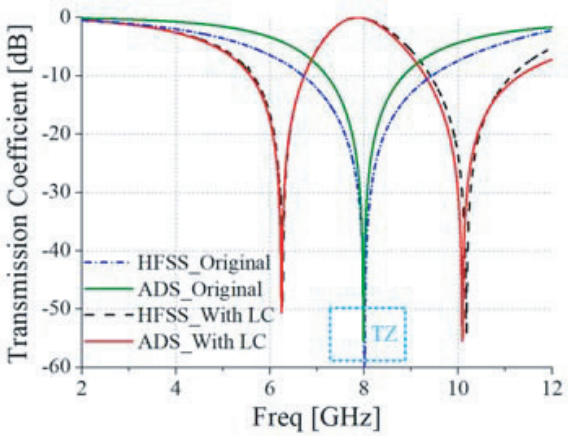

Figure 3. Simulated results of TTTG from *HFSS* and *ADS*.

An equivalent circuit model (ECM) is developed to explain this electromagnetic response. According to Munk's theory in [7], the ECM of TTTG under normal incidence is illustrated in Fig. 2(a), where $Z_0 = 377\,\Omega$ is the free-space characteristic impedance, $Z_T = Z_0/\sqrt{\varepsilon_r}$ the characteristic impedance of dielectric substrate, L the equivalent inductance, and C the equivalent capacitance. However, when parallel LC resonators are loaded in the structure, the ECM of TTTG will change into two series LC circuits arranged in parallel and then in series with the LC resonator, as shown in Fig. 2(b), where the series L_rC_r circuit is extracted from the structure identified in the rectangular dotted line, and the series L_eC_e circuit is from the structure identified by the circular dotted line. The values of equivalent inductance and capacitance in the models can be approximately calculated using formulas (1) and (2) from [19]. To make the results obtained from the circuit models agree well with that from the full-wave simulation and get more accurate values of the inductances and capacitances, these circuits are modeled and optimized in *ADS*. Conclusive results are plotted in Fig. 3. As can be seen, a good agreement is obtained.

$$L = \mu_0\mu_{eff}\frac{D}{2\pi}\ln\left(\csc\left(\frac{\pi w}{2D}\right)\right) \tag{1}$$

$$C = \varepsilon_0\varepsilon_{eff}\frac{2D}{\pi}\ln\left(\csc\left(\frac{\pi g}{2D}\right)\right) \tag{2}$$

where D is the periodic size of the TTTG unit cell, g the gap between two units, w the width of girds, μ_0 the free-space permeability, ε_0 the free-space permittivity, μ_{eff} the effective permeability, ε_{eff} the effective permittivity, and $\varepsilon_{eff} = (\varepsilon_r + 1)/2$.

2.2. Design of Bandpass FSS

BPFSS plays an important role in the design of FSA. The performance requirements of BPFSS include low insertion loss in passband and polarization insensitivity as well as angular stability. To meet these requirements, a complementary FSS [20] is proposed and investigated, as shown in Fig. 4. It is composed of star-shaped patches and a capacitive surface with star-shaped apertures. Both the patches and the capacitive surface are mounted on the top surface of a thin substrate with a relative permittivity of 3.5 and thickness of 0.5 mm. The other geometrical parameters are set as $lx = 15$ mm, $ly = 10$ mm, $cx = 2.5$ mm, $cy = 1.6$ mm. Fig. 5 shows the simulation results of the proposed BPFSS. As can be seen, it has a bandpass response at the frequency of 7.8 GHz with the insertion loss being 0.05 dB. In addition, the performance can be maintained well when the incident angles range from 0° to 45° for both TE and TM polarizations.

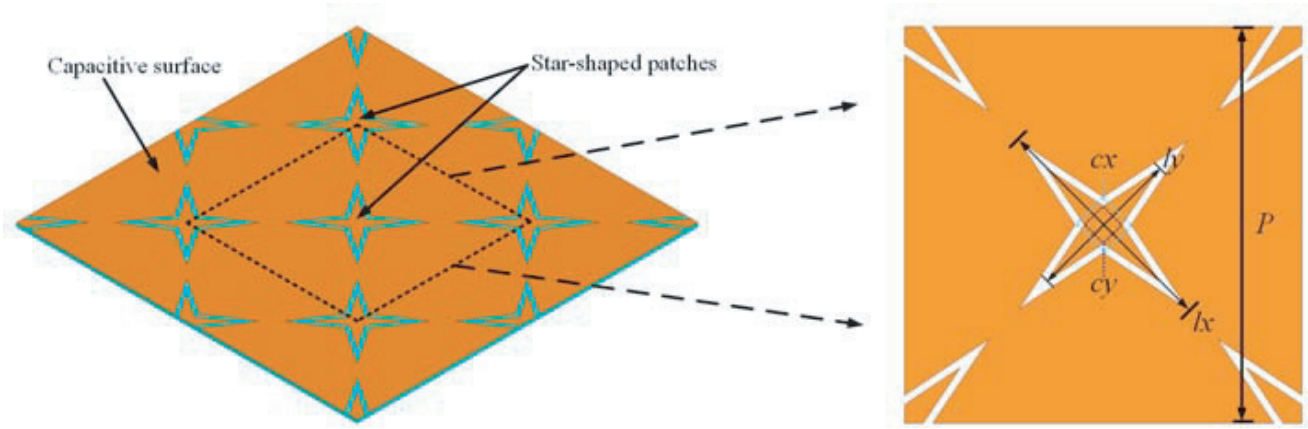

Figure 4. 3-D prospect view of structure and detailed unit cell of BPFSS.

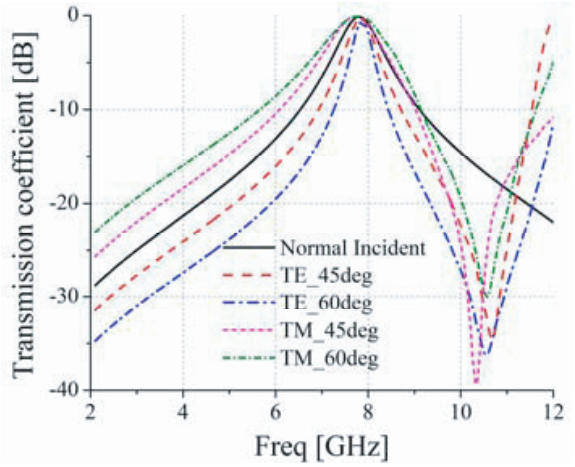

Figure 5. Simulated results under different incident angles for TE and TM polarizations.

2.3. Realization of FSA

In addition to the transmission characteristic, FSA should also have a good absorption ability. Therefore, the choice of suitable resistor is also very important. It should conform to the principles of designing CCA and is commercially available. In this paper, the values of these resistors are finally determined by using software *HFSS* to achieve the best reflection coefficient reduction and bandwidth enhancement

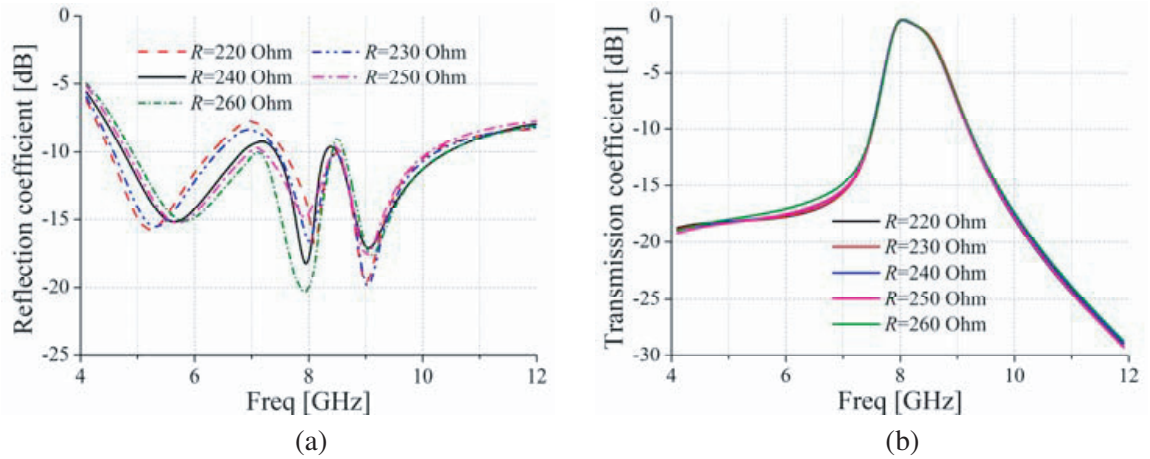

Figure 6. Effect of resistances on (a) reflection coefficient and (b) transmission coefficient.

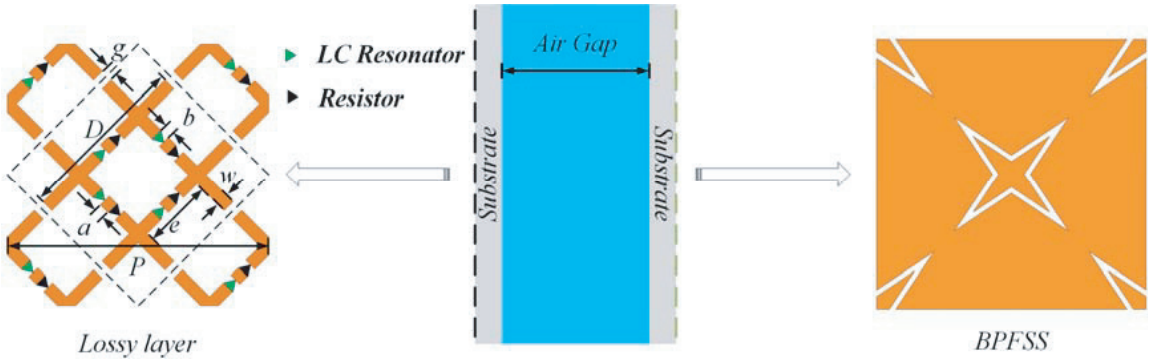

Figure 7. Structure of the designed FSA. $P = 25\,\text{mm}$, $D = 16.5\,\text{mm}$, $e = 6.8\,\text{mm}$, $g = 1.2\,\text{mm}$, $w = 1.2\,\text{mm}$, $a = 1.0\,\text{mm}$, $b = 0.4\,\text{mm}$.

while the transmission characteristic should not be influenced. Fig. 6 shows the simulated results under different resistances. It can be seen that the best performance will be obtained when resistance is chosen as 240 ohm.

With determination of all parameters, the final structure of FSA is as shown in Fig. 7. There are four sets of parallel LC resonators and resistors in each TTTG unit. They are arranged in four-fold symmetry. Both TTTG and BPFSS are printed on the surface of an F_4BM350 substrate with the relative permittivity of 3.5 and thickness of 0.5 mm. The air gap between these two layers is calculated about a quarter of substrate wavelength regarding to 8 GHz.

3. PERFORMANCE OF PROPOSED FSA

3.1. Absorption and Transmission Characteristic

Simulated reflection and transmission coefficients of the proposed FSA under transverse electronic (TE) and transverse magnetic (TM) polarizations with various incident angles are plotted in Fig. 8. As can be seen, it shows a bandpass response at the frequency of 8.02 GHz under normal incident, with insertion loss being 0.2 dB and -3 dB fractional bandwidth being about 10%. Over the bands from 4.76 GHz to 7.49 GHz and from 9.23 GHz to 10.57 GHz, both transmission and reflection coefficients are under -10 dB, which indicate good absorption in these frequency bands. In addition, the performance is maintained well with the incident angles up to 45° for both TE and TM polarizations. However, as the incident angles continue increasing, the absorbing ability becomes poor. One probable reason may

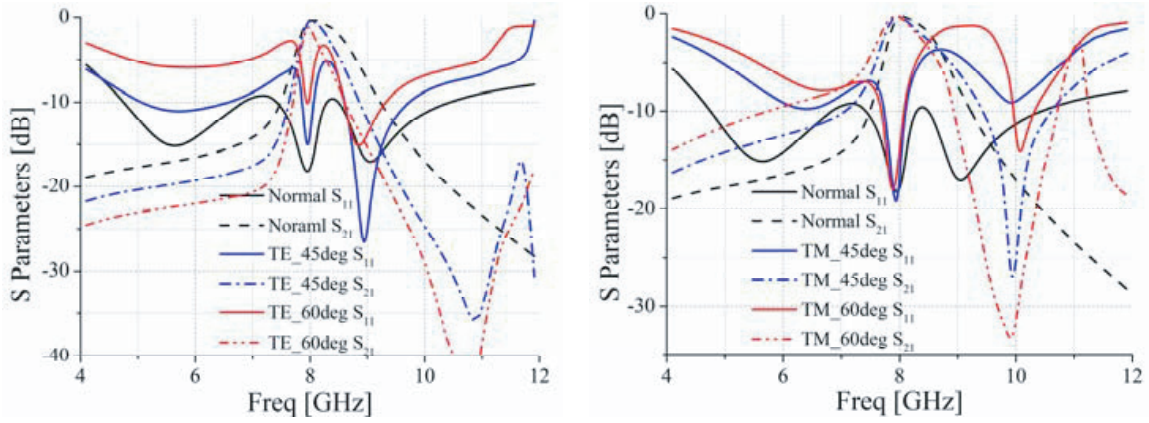

Figure 8. Simulated reflection and transmission coefficients under different incident angles for (a) TE polarization and (b) TM polarization.

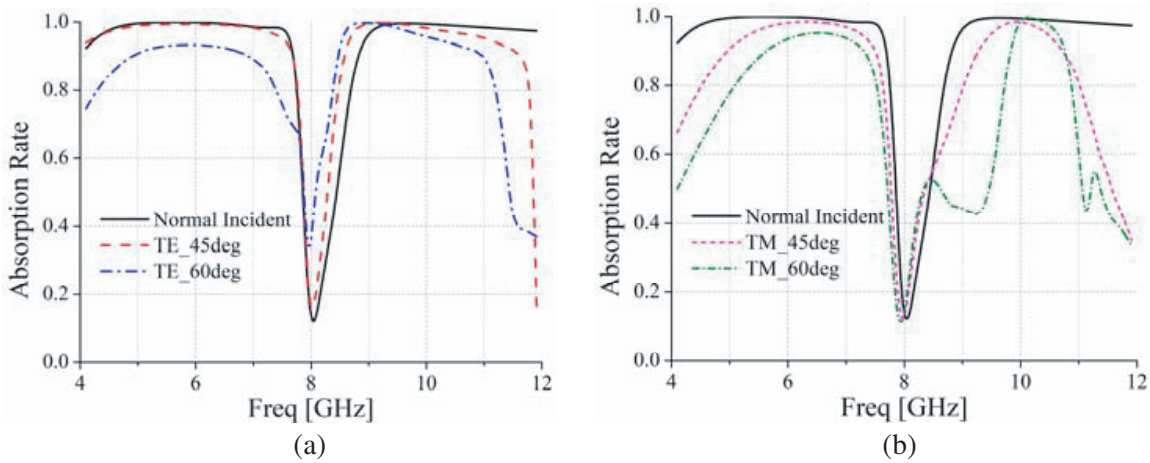

Figure 9. Calculated absorption under different incident angles for (a) TE and (b) TM polarization.

be that no miniaturization has been taken into consideration during designing process.

In order to illustrate the performance more concisely and intuitively, absorption rate is also calculated using formula (3), and the obtained results are plotted in Fig. 9.

$$Absorption{=}1 - mag\,(S_{11})^2 - mag\,(S_{21})^2 \tag{3}$$

3.2. Application in Bistatic RCS Reduction

To illustrate the advantage of FSA over BPFSS in bistatic RCS reduction, the same size FSA and BPFSS (250 mm × 250 mm) are simulated in *HFSS*. Fig. 10 shows the simulated results as a function of bistatic angle at 9.5 GHz, where vertical polarization refers to $\theta = 0^0, \varphi = 0^0$ while horizontal polarization refers to $\theta = 0^0, \varphi = 90^0$ in a spherical coordinate system. As can be seen, the proposed FSA has a lower bistatic RCS than BPFSS at all observed bistatic angles. In addition, when the bistatic angle is equal to 0°, the RCS reduction can be up to 12.5 dB, which indicates that a good monostatic RCS reduction can also be obtained.

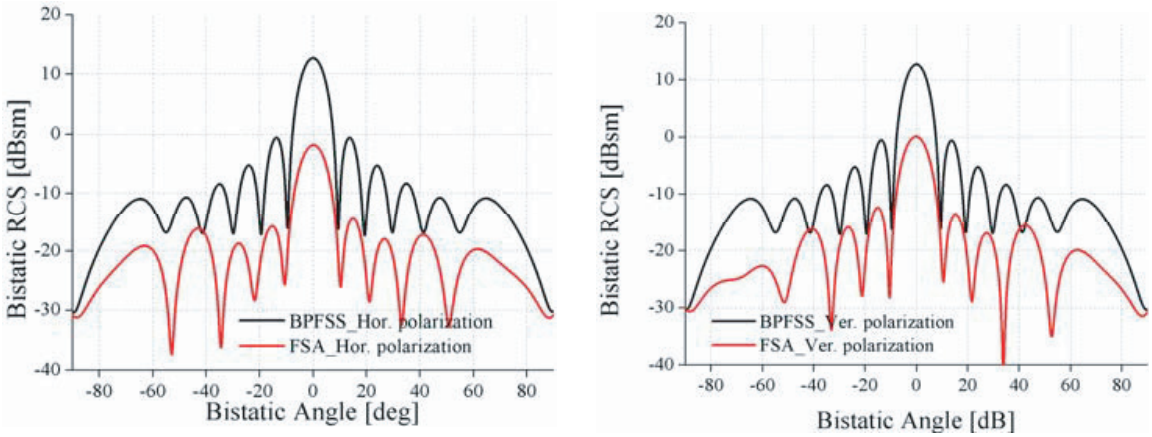

Figure 10. Bistatic RCS comparison of FSA and BPFSS for (a) vertical and (b) horizontal incident plane waves at 9.5 GHz.

4. EXPERIMENT RESULTS AND DISCUSSION

An FSA prototype is also fabricated using the printed circuit board (PCB) technology to verify this method in this paper. The overall size of this prototype is 250 mm × 250 mm, on which 400 sets of parallel LC resonators and resistors are soldered using surface-mount technology (SMT), as shown in Fig. 11(a). All the lumped components utilized in fabrication are with 0402 packages and produced by Murata Company. Meanwhile, plastic nuts and bolts are fixed in the four corners of prototype to maintain the necessary air gap between these two substrates.

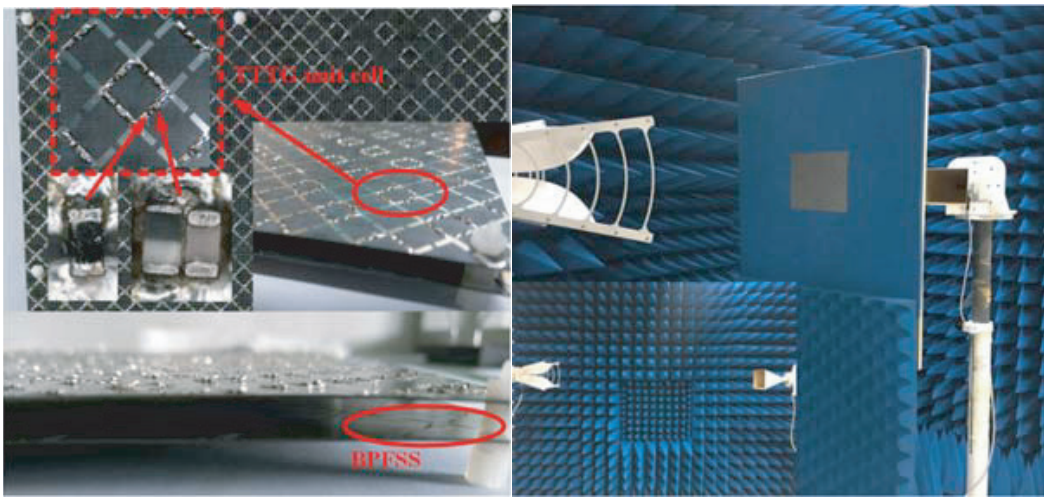

Figure 11. Pictures of fabricated FSA in (a) and measurement system in (b).

The prototype is measured in a microwave anechoic chamber under the guidance of free space measurement setup, as shown in Fig. 11(b). Two standard horn antennas are aligned for calibration first, and then the proposed FSA is fixed at the neutral of these two horns. The values of reflection and transmission coefficients can be read from the R&G vector network analyzer. Since the background noise is too strong, the obtained results are processed in Matlab, as shown in Fig. 12. It can be seen that the measured resonant frequency is about 8.14 GHz, slightly higher than the simulated 8.02 GHz.

Over the bands from 4.5 GHz to 7.5 GHz and from 9.1 GHz to 11.3 GHz, both measured transmission and reflection coefficients are under −10 dB, which agree well with simulations. However, the measured insertion loss at the resonant frequency is 2.4 dB, which deteriorates seriously compared to the simulated 0.2 dB. This discrepancy is mainly caused by the ohmic losses from lumped components, which are regarded as lossless in simulation. The deformation of geometry caused by the change of air gap may be another factor. Beyond that, the errors brought by the signal processing in Matlab cannot be neglected. However, these issues are not insurmountable. By selecting low-loss lumped components and adopting optimized processing algorithm, the errors caused by lumped components and signal process can be

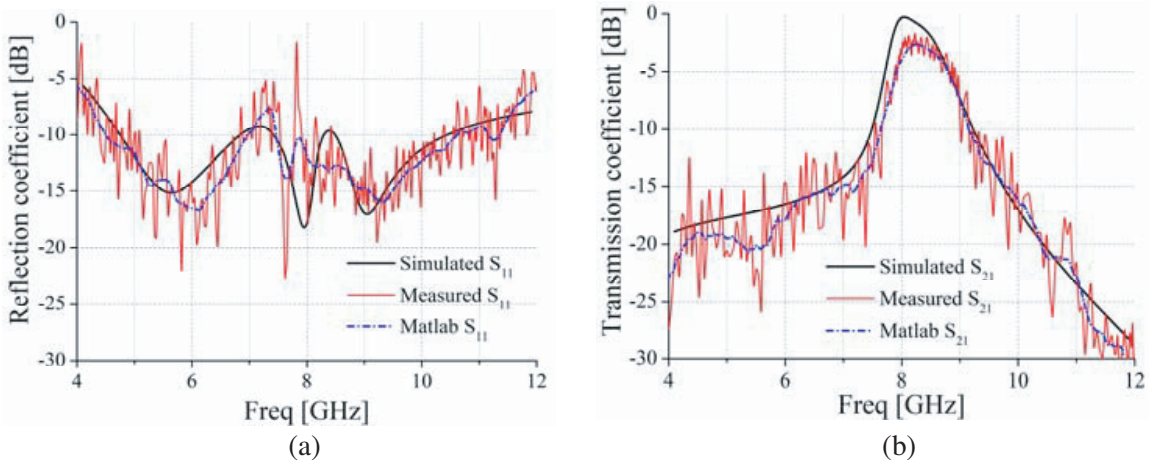

Figure 12. Simulated and measured results of (a) reflection and (b) transmission coefficients.

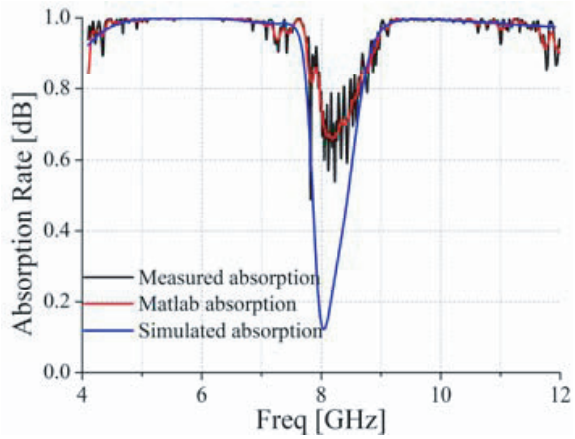

Figure 13. Absorption rate calculated from simulated and measured results.

Table 1. Performance comparison of the designed FSS with the state-of-the-art.

Ref.	Insertion loss (dB)	Lower absorption (GHz)	Upper absorption (GHz)	Oblique incidence
[16]	0.26	2.1–4.1	5.3–11.4	No refers
[17]	0.92	1.5–2.7	4.5–5.8	40°
[18]	0.29	2.8–4.2	8–9	30°
This work	0.2	4.7–7.5	9.2–10.6	45°

reduced. The deformation problems can be ameliorated by using foam with a permittivity close to 1 instead of plastic nuts and bolts.

The large insertion loss in turn leads to the measured absorption rate in passband bigger than that from the simulation, as shown in Fig. 13. Anyway, the method is verified well.

The performance of the proposed FSA is also compared with the state-of-the-art in Table 1, where the absorption band is defined as $S_{11} < -10\,\text{dB}$ and $S_{21} < -10\,\text{dB}$. It can be seen from Table 1 that the proposed FSA has the lowest insertion loss as well as the best angular stability in all of these structures.

5. CONCLUSION

In this paper, a method of designing the FSA which has a transmission band between two neighboring absorption bands is presented and investigated. It is implemented by constructing parallel LC resonators in the unit cell. The advantage of this method over previous approaches is that no additional bias network is required to mount the lumped components. An equivalent circuit model is developed for a better understanding of this method. Meanwhile, a prototype was fabricated and measured. The measured and simulated results are in good agreement and verify the method well. In addition, the proposed FSA demonstrates a low sensitivity with respect to the polarization of incident EM waves and has a stable performance when the incident angles are up to 45°, which indicates that it could be widely used in practice.

ACKNOWLEDGMENT

This work was supported by the National Basic Research Program of China-973 program 2015CB857100, National Natural Science Foundation of China (No. 61401327, 61471278, 61601350), the Foundation of Chinese Academy of Space Technology (CAST 2015-11), and Natural Science Basic Research Plan in Shaanxi Province of China (No. 2015JQ6217).

REFERENCES

1. Ghosh, S. and K. Srivastava, "Broadband polarization-insensitive tunable frequency selective surface for wideband shielding," *IEEE Trans. Electrom. Compat.*, Vol. 60, 166–172, 2018.
2. Orr, R., V. Fusco, et al., "Circular polarization frequency selective surface operating in Ku and Ka band," *IEEE Trans. Antennas Propag.*, Vol. 63, 5194–5197, 2015.
3. Vallecchi, A., R. J. Langley, and A. G. Schuchinsky, "Metasurfaces with interleaved conductors: Phenomenology and applications to frequency selective and high impedance surfaces," *IEEE Trans. Antennas Propag.*, Vol. 64, 599–608, 2016.
4. Baskey, H. B. and M. J. Akhtar, "Design of flexible hybrid nanocomposite structure based on frequency selective surface for wideband radar cross section reduction," *IEEE Trans. Microw. Theory Techn.*, Vol. 65, 2019–2029, 2017.
5. Zheng, J. and S. J. Fang, "A new method for designing low RCS patch antenna using frequency selective surface," *Progress In Electromagnetics Research Letters*, Vol. 58, 125–131, 2016.
6. Joozdani, M. Z., M. K. Amirhosseini, and A. Abdolali, "Wideband radar cross-section reduction of patch array antenna with miniaturized hexagonal loop frequency selective surface," *Electronics Letters*, Vol. 52, 767–768, 2016.
7. Munk, B. A., *Frequency Selective Surfaces: Theory and Design*, Wiley, New York, NY, USA, 2000.
8. Yi, B., L. Yang, and P. Liu, "Design of miniaturized and ultrathin absorptive/transmissive radome based on interdigital square loops," *Progress In Electromagnetics Research Letters*, Vol. 62, 117–123, 2016.
9. Munk, B. A., "*Metamaterials: Critique and Alternatives*, Wiley, Hoboken, NJ, USA, 2009.
10. Chen, Q. and L. Liu, "Absorptive frequency selective surface using parallel LC resonance," *Electronics Letters*, Vol. 52, No. 6, 418–419, 2016.

11. Li, A., J. H. Fu, Z. F. Wang, W. Chen, L. Bo, and C. He, "An absorptive/transmissive radome based on metamaterial," *IEEE Int. Conf. on Electronic Information and Communication Technology*, 596–598, Harbin, China, August 2016.
12. Chen, Q., S. Yang, et al., "Design of absorptive/transmissive frequency-selective surface based on parallel resonance," *IEEE Trans. Antennas Propag.*, Vol. 65, 4897–4902, 2017.
13. Yu, D., P. Liu, Y. Dong, et al., "Active absorptive frequency selective surface," *Electronics Letters*, Vol. 53, 1087–1088, 2017.
14. Yi, B., P. Liu, C. Yang, et al., "Analysis of absorptive and transmissive radome," *IEEE International Symposium on Microwave, Antenna, Propagation and EMC Technologies*, 616–619, 2015.
15. Yu, Y., Z. Shen, T. Deng, et al., "3-D frequency-selective rasorber with wide upper absorption band," *IEEE Trans. Antennas Propag.*, Vol. 65, 4363–4367, 2017.
16. Omar, A., Z. Shen, and H. Huang, "Absorptive frequency-selective reflection and transmission structures," *IEEE Trans. Antennas Propag.*, Vol. 65, 6173–6178, 2017.
17. Han, Y. and W. Che, "Switchable low-profile broadband frequency-selective rasorber/absorber based on slot arrays," *IEEE Trans. Antennas Propag.*, Vol. 65, 6998–7008, 2017.
18. Huang, H. and Z. Shen, "Absorptive frequency-selective transmission structure with square loop hybrid resonator," *IEEE Antennas Wireless. Propag. Lett.*, Vol. 16, 3212–3215, 2017.
19. Abadi, S. M. A. M. H., J. H. Booske, and N. Behdad, "Exploiting mechanical flexure as a means of tuning the responses of large-scale periodic structures," *IEEE Trans. Antennas Propag.*, Vol. 64, 933–943, 2016.
20. Jiao, J., N.-X. Xu, X. G. Feng, et al., "Tunable complementary frequency selective surfaces based on cross-elements," *Guangxue Jingmi Gongcheng/Optics & Precision Engineering*, Vol. 22, 1430–1437, 2014.